Crystallographic characterization of a BFMO layer grown on STO through HRTEM imaging and simulation

Author: Nikolas Deco.
Advisors: Francesca Peiró Martínez and Catalina Coll Benejam
Facultat de Física, Universitat de Barcelona, Diagonal 645, 08028 Barcelona, Spain.

Abstract: $Bi(Fe_{0.5}Mn_{0.5})O_3$ is a multiferroic material with electric and magnetic properties of great interest for potential spintronic applications. To understand what triggers its peculiar behaviour it is essential to know its structure, and for that, TEM is the ideal tool for analysis at the nanoscale. The aim is to study a thin film of BFMO grown on a STO substrate through the analysis of high resolution transmission electron microscopy (HREM) images and the use of HREM simulations from theoretical atomistic models built also in this project. The results show that this method can lead to useful results in structure determination of a material.

I. INTRODUCTION

Multiferroic materials are of great interest mainly because of the coexistence of magnetism and ferroelectric phenomena, which lead to interesting applications in device control using both magnetic and electric phenomena [1], for instance, data storage and multifunctional devices show up as an interesting research line [2]. $Bi(Fe_{0.5}Mn_{0.5})O_3$ (BFMO) in particular, is a multiferroic material with some very promising characteristics regarding to its magnetoelectric properties that seem suitable for spintronic and magnonic applications. [3]

To understand the functional behaviour of this material, it is mandatory to know well the structural configuration when grown as thin layer on a substrate. To perform a crystallographic characterization with high spatial resolution, Transmission Electron Microscopy turns out to be the ideal tool to resolve the atomic structure. [4]

The main purpose of this work will be to characterize a thin layer of BFMO grown on $SrTiO_3$ (STO), determining its crystalline phase and structural configuration, as well as to show how it has epitaxially grown over the substrate. To do so, indexing diffraction spots in reciprocal space and phase contrast high resolution transmission electron microscopy image simulation is a suitable combination of tools. In this way, we will be able to localize and identify the different atomic planes seen in the images and hence determine the whole structure's conformation.

II. EXPERIMENTAL DETAILS

A. Sample growth

For the BFMO sample growth, films of around 43 nm were deposited by a KrF excimer laser focusing a stoichiometric ceramic target with a bismuth excess of 10%. The samples were grown on a $SrTiO_3$ (100) substrate at a temperature of 650 ºC, and with an oxygen pressure of 0.6 mbar, ablation rate of 5 Hz and laser fluency at approximately 1.7 J cm^{-2}. More details about sample growth can be found in reference [3].
For TEM examination, we necessarily have to mechanically thin the sample to make it electrotransparent. The mechanical cross section preparation is ideal if we want to have access to the interface between the layers. The sample is cut in two pieces and glued up with the active layers facing each other, it is then polished and finally submitted to Ar+ ion beam etching.
The sample is bombarded at a low angle in order to create a hole in the central region, creating areas around this hole thin enough for optimal observation as shown in FIG. 1.[4]

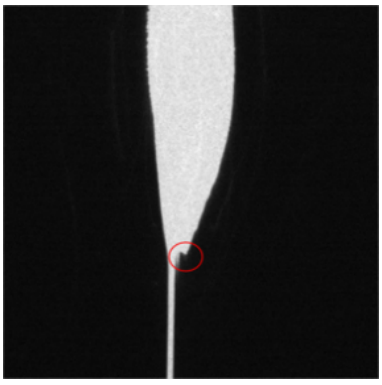

FIG. 1: Low magnification image of a thin region of the prepared sample, where the diffraction electron images were taken.

High resolution images and electron diffraction patterns were acquired using a Jeol 2010F instrument equipped with a field emission gun and operated at 200kV, in the Scientific and Technical Centers of the University of Barcelona (CCiTUB).

*Electronic adress: nikodeco8@gmail.com

B. High resolution transmission electron microscopy (HREM) and electron diffraction

High Resolution TEM (HREM) is an imaging technique to obtain phase contrast images. To be able to use this mode of operation the material has to be between 20-50 nm of thickness.

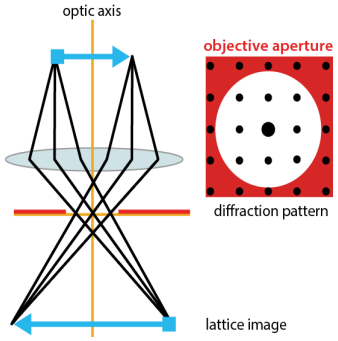

FIG. 2: Schematic of the beams trajectory when using the microscope to obtain high resolution images. [6]

The incident parallel electron beam is first scattered and diffracted by the crystalline specimen. The outgoing radiation goes through an objective lens, which function is focusing the beams on the back focal plane of the lens, this is, in fact, the electron diffraction pattern, and also a primary enlarged image of the sample is formed at the image plane of the lens. This primary image is used by the rest of the lens, which magnify it to form the final image. HREM mode needs the objective aperture in the back focal plane to be big enough to be able to use multiple diffracted beams as well as the direct one, so that interferences of all those waves will project an image of the crystalline lattice, revealing the atomic positions. [4], [5]
A Fast Fourier Transform (FFT) to the HRTEM image can be computed which retrieves the diffraction pattern.
Given a cubic, tetragonal or orthorhombic cell with a particular lattice parameter and a spot in the diffraction pattern represented by its Miller indexes, the distance between the planes with these indexes is given by:

$$\frac{1}{d^2} = \frac{h^2}{a^2} + \frac{k^2}{b^2} + \frac{l^2}{c^2} \qquad (1)$$

where d represents the interplanar spacing, h, k and l are the Miller indexes, and a, b and c stand for the lattice parameters in the three orthogonal directions of the crystal's axes. [7]

C. Simulation

To simulate HRTEM images we will use an open source simulation software called TEMSIM, by E.J. Kirkland. TEMSIM is based on the multislice approach, that calculates the propagation of the incident electron wave through a sliced atomic model of the object considered as a periodic potential and then convolves the outgoing resulting electron wave with the contrast transfer function that describes the objective system of the microscope. [8]

The multislice approach is a popular method in the theory of transmission electron microscope image calculation of thick specimens. It takes into account the effects of plural scattering in the specimen as well as its extension along the optic axis of the microscope. In this approach the structure is divided into thin slices where the electron beam is alternately transmitted and propagated. Each slice has to be thin enough to be a weak phase object, which means that the electron beam wave's amplitude remains constant when going through this layer, while the phase is slightly changed.

Setting up the initial value of the wave function $\psi(x,y)$ in an x, y plane, the electron wave function through the specimen is recursively calculated along the z direction applying the multislice equation, which in compact form can be written as:

$$\psi(x,y) = p_n(x,y,\Delta z_n) \otimes [t_n(x,y)\psi(x,y)] + \mathcal{O}(\Delta z^2)$$

Where t_n and p_n stand for the transmission and propagation operators in the n-slice at a certain depth;

$$t(x,y,z) = exp\left[i\sigma \int_z^{z+\Delta z} V(x,y,z')dz'\right]$$

$$p(x,y,\Delta z) = FT^{-1}[P(k,\Delta z)] = \frac{1}{i\lambda\Delta z} exp\left[\frac{i\pi}{\lambda\Delta z}(x^2+y^2)\right]$$

where $V(x,y,z)$ is the atomic potential, λ and k are the wavelength and wavenumber, respectively, of the electron wave, Δz is the depth of the specimen and $P(k,\Delta z)$ is the propagator function,

$$P(k,\Delta z) = exp(-i\pi\lambda k^2 \Delta z)$$

Finally, the wave function has to be convolved with the Point Spread Function that contains all the information about the microscope, as aberrations, defocus, etc. [9]

TEMSIM uses this approach to simulate HRTEM images from a given unit cell or structure of a certain material, and with the microscope parameters that are used to describe its characteristics or operation mode (acceleration voltage, convergence semiangles, diffraction aperture diameter and aberration coefficient). Changing successively some other parameters as the defocus of the objective lens and the possible sample thickness, the images are simulated in order to fit as much as possible the experimental images.

EJE Z and RHODIUS software packages, available in a server at the Group of Nanomaterials and Catalysis, Laboratory of the University of Cádiz are used to build atomistic models with the crystallographic phases of the material we want to use in the simulation. [10]. When we have chosen the structure we want to simulate, we can obtain the file that gives us the unit cell of a given phase of the material, or even an extended layer built up with this unit cell.

III. RESULTS

A. Structure and composition

Our sample consists of a BFMO thin foil with an experimental thickness of ≈57 nm, which is higher than the nominal value, prepared as a thin layer laying on a STO substrate.

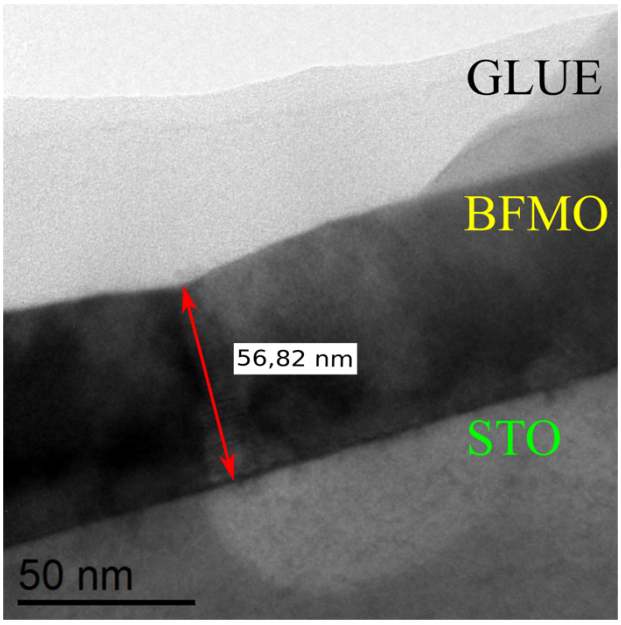

FIG. 3: Low magnification image of the BFMO thin film of 56,82 nm on top of STO substrate. On top of BFMO the glue of the preparation can be seen.

FIG. 3 corresponds to a low magnification image that shows a cross section view of the sample. If we zoom in into our region of interest the interface between the BFMO layer and the STO substrate is viewed at atomic resolution as presented in FIG. 4 a).

Let us start with the characterization of the STO substrate, a material with perovskite type structure, generally described by ABO_3 formula, where A ion (in our case Sr) is twelve fold coordinated by oxygen (like a dodecahedra) and B ion (Ti in our case) is octahedrally coordinated by oxygen ion. To corroborate this crystalline structure and identify the orientation of visualization of the substrate, namely the zone axis, we must first calculate the FFT of a selected area of our image. The FFT of a selected region on the substrate is seen in the inset of FIG .4. In fact, this FFT is a power spectrum of the HREM image that retrieves the electron diffraction pattern, that we also acquired using a selected area diffraction mode.

The second step is to determine the interplanar distance by measuring the distance and angles of the spots appearing on the FFT, and compare them with the theoretical values of the reported STO structure in the 221 space group which corresponds to a perovskite cubic phase with a lattice parameter of 3.942 Å [11]. We can then tag each spot of the FFT by its Miller index, meaning that we identify each spot as a specific family of planes of the atomic lattice, as labelled in FIG. 4 c). The zone axis, parallel to the electron beam, is then obtained from the cross product of two non aligned vectors of the reciprocal space. For a cubic symmetry, all <100> planes are equivalent and, in this case, we have used the [0 0 1] zone axis.

We can do a similar analysis on the electron diffraction pattern. The interplanar distances corresponding to these experimental measurements are shown in the second column of TABLE I, and the indexation of the spots is seen in FIG. 4 d)

If the HREM is well calibrated, we can also measure the interplanar distances in real space, as seen in FIG. 4 b) and the results are presented in the first column of TABLE I.

The theoretical values obtained in the crystallographic analysis using the EJE Z software package [10], that uses the general formula of Equation (1) to compute distances from the Miller indexes, are also included in the third column of TABLE I. for comparison.

	Real space (Å)	Electron diffraction(Å)	Theoretical (Å)
(1 -1 0)	2.626	2.690	2.785
(1 1 0)	2.641	2.695	2.785
(0 1 0)	3.980	3.811	3.940

TABLE I. Comparison of the mean interatomic distances obtained experimentally, and those obtained in the analysis of the theoretical structures for STO.

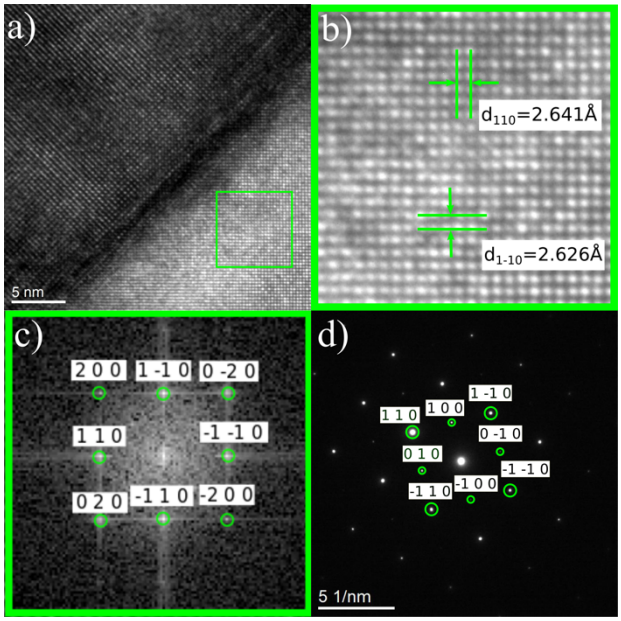

FIG. 4: a) High magnification image of the STO and BMFO interface with the squared region we further analyse. b) Squared region from a) where interplanar distance have been measured through profile analysis. c) FFT of the squared region in a) with the indexed spots. d) Electron diffraction image with its spots indexed.

A similar analysis procedure can be carried out for the BFMO thin film. However, we don't know which the phase of the BFMO is a priori. Our sample has been grown in the form of a specific type of perovskite with the general formula $A_2BB^*O_6$., where in our case A cation

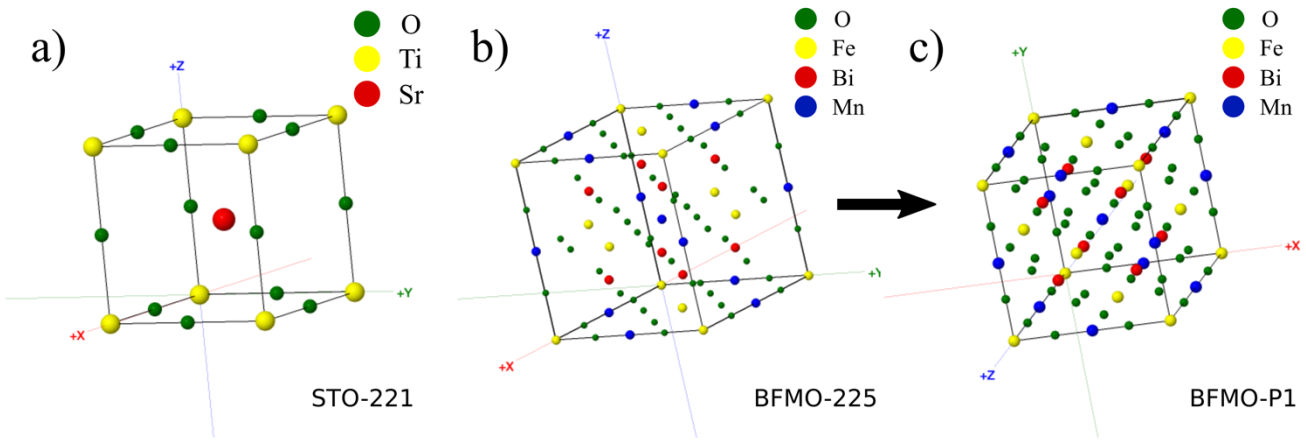

FIG. 6: a) Representation of the STO cell used in the simulations, b) BFMO cell in the 225-space group with cubic symmetry c) BFMO in the new P1 phase we created with tetragonal symmetry.

sites are occupied with bismuth (Bi) and B sites with Iron (Fe) and manganese (Mn). Previous X-ray diffraction (XRD) experiments on our sample revealed a tetragonal cell configuration with the lattice parameters a=b=5.5500 Å and c=7.9999Å. Using the open source software SPuDS [12] we can inquire its symmetry group. The software is able to suggest the most probable disposition of the atoms in the cell taking into account its stoichiometry and the elements, with their respective oxidation number, constituting the structure, as well as imposing it to find the simplest symmetry possible. The result is a BFMO cell in the 225-space group, which is a cubic cell as well, with lattice parameter a = 8.6738 Å, and 4 non-equivalent atoms needed to build the asymmetric unit cell. The lattice parameters are forced to be the ones obtained in the X-ray diffraction. To do so, we have to break its symmetry, transferring the relative position of every atom to the orthorhombic new cell with 40 non-equivalent atoms.

Both BFMO phases can be seen in FIG. 5 b) and c), where the STO cubic perovskite unit cell has been also included for comparison. Now that we know the BFMO symmetry, we can follow the same process we did with STO, to index the spots appearing in the FFT (FIG 6 c)) or from the experimental diffraction patterns (FIG 6 d)). We then measure the mean interatomic distances obtained for different planes, see FIG. 6 b) and compare them with the theoretical values, as presented in TABLE II. We find that the one that fits best is the [0 0 1] zone axis of BFMO-P1, We can also conclude that the relation of epitaxy is $(110)[001]_{BFMO}//(100)[001]_{STO}$

	Real space (Å)	Electron diffraction(Å)	Theoretical (Å)
(1 1 0)	2.765	2.840	2.970
(1 -1 0)	2.742	2.820	2.970
(0 1 0)	4.098	4.060	3.920

TABLE II. Comparison of the mean interatomic distances obtained from the real space and electron diffraction images of two different zones, and those obtained in the analysis of the theoretical structures.

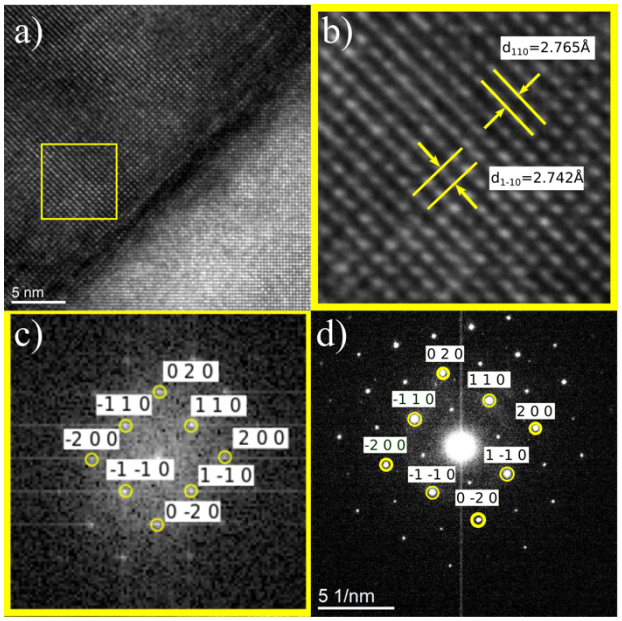

FIG. 5: a) High magnification image of the sample with the squared analysed region. b) Squared region in a) with interplanar distances measured through profile analysis. c) FFT of the squared region in a) with its indexed spots. d) Electron diffraction image of the BFMO layer with its indexed spots.

B. Simulation

Theoretical simulations of HREM images from atomistic models built according to the crystalline structure previously determined (cubic perovskite for STO a = 3.942 Å and tetragonal for BFMO with a=5.5500 Å and b=c=7.999 Å) can be used to verify that the assumed structures are correct.

The simulation parameters were set similar to the experimental ones, being the incident energy beam 200 keV, the image size 2048 px in both x and y directions, the slice thickness 2 Å, spherical aberration C_s3 and C_s5 0.5 and 0, objective aperture size 12 mrad, the illumination semiangle 0.8 mrad and finally the defocus spread 90 Å. STO and BFMO thickness and defocus have been selected by trial and error arriving to an optimal simulated image that fits the experimental ones.

To prove that the structures we found are the ones corresponding to the experimental images, we superpose our simulations results with the experimental image and compare both experimental and simulated structures, see FIG. 7.

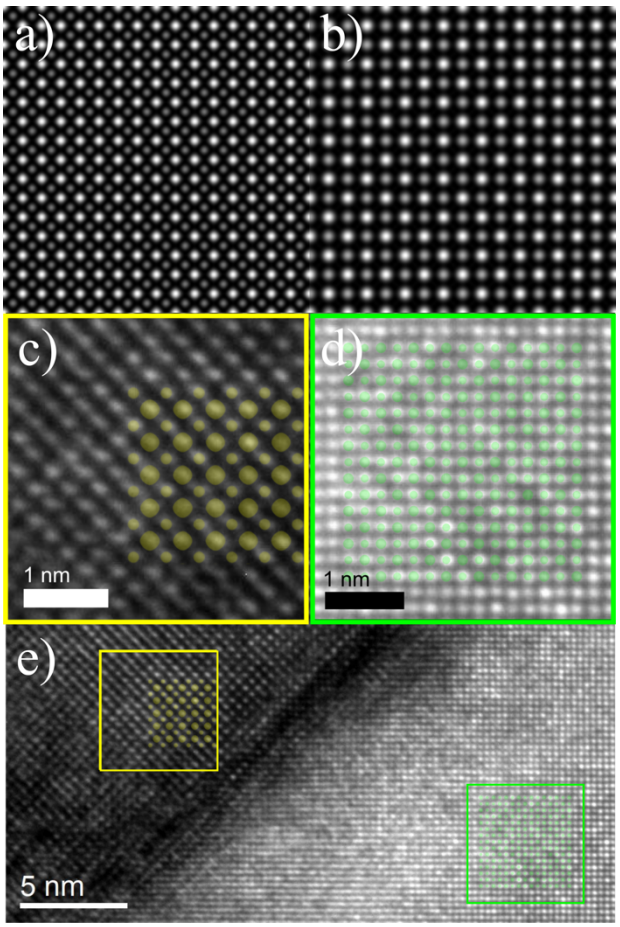

FIG. 7: a) BFMO lattice simulated with sample thickness and defocus spread respectively; t=40nm d=100Å b) STO lattice simulated with t=16nm d=1200Å. c) Superposition of the simulated BFMO image with its corresponding experimental image. d) Superposition of the simulated STO image with the experimental one. e) General view of the high magnification image of the interface with simulated lattice superposed.

IV. DISCUSSION

In summary, for both STO and BFMO materials, the interplanar distances were obtained by three different ways. In comparison with the theoretical values from Equation (1), we have found errors of 5-6% in the STO case, and errors up to 7% in the BFMO case. These differences can arise from a slightly different calibration of the imaging and diffraction modes in the microscope, added to the experimental errors.

Also, BFMO structure is not totally ensured to be the one that we assumed. We used the phase that best described our results, but these is not a known result as it is for STO. Regarding the simulations, the superposition of the simulated images fit greatly the experimental images.

V. CONCLUSIONS

We have used real space and electron diffraction images using HREM technique. Analysing them, we have found the zone axis for both layers, the phase for STO, and the most probable phase for BFMO. We have also determined the direction of the sample growth; the [1 1 0] for BFMO and the [1 0 0] for STO.
Superposing the HREM simulated images with the experimental ones we have corroborated that our assumptions made after the characterization process were accurate.

VI. ACKNOWLEDGMENTS

I would like to express my sincere gratitude to my advisor Dr. Francesca Peiró for her guidance and advises. Also, I am especially grateful for the assistance and constant support of Catalina Coll who helped me in carrying out this work and for Javier's Blanco help in the experimental field.

VII. REFERENCES

[1] L. Zhao *et al.*, "Mn $_3$ TeO $_6$ - a new multiferroic material with two magnetic substructures," *Phys. status solidi - Rapid Res. Lett.*, vol. 9, no. 12, pp. 730–734, Dec. 2015.
[2] W. Ren, "Nanodots of multiferroic oxide material BiFeO3 from the first principles," *Adv. Manuf.*, vol. 1, no. 2, pp. 166–175, Jun. 2013.
[3] E. Coy, I. Fina, K. Zał ̨eski, A. Krysztofik, L. Yate, L. Rodriguez, P. Graczyk, H. Głowi´nski, C. Ferrater, J. Dubowik, and M. Varela, High-temperature magnetodielectric $Bi(Fe_{0.5}Mn_{0.5})O_3$ thin films with checkerboard-ordered oxygen vacancies and low magnetic damping
[4] David B. Williams and C. Barry Carter, Transmission Electron Microscope: A Textbook for Material Science, Springer, New York, 2nd. edition, 2009.
[5] Lluís López Conesa, PhD. Thesis, Advanced TEM Imaging Tools for Materials Science, University of Barcelona, 2015.
[6] Mycroscopy Australia. TEM, Image formation basics. https://myscope.training/legacy/tem/background/concepts/imagegeneration/detail.php#panel
[7] John M. Cowley, Diffraction physics, Elsevier, Amsterdam, 3rd. edition, 1995.
[8] Earl J. Kirkland, Temsim software, http://people.ccmr.cornell.edu/ ~ kirkland/
[9] Earl J. Kirkland, Advanced Computing in Electron Microscopy, Springer, New York, 2nd edition, 2010.
[10] D. J. Perez-Omil, Ph.D. thesis, University of Cadiz, Spain, 1994. Interpretación sistemática de imágenes de microscopia electrónica de alta resolución de materiales policristalinos. Estudio de catalizadores metálicos soportados.
[11] Alastair G. Hartley Smith, PhD. Thesis,
Structural and Defect Properties of Strontium Titanate, University College London, 2011.
[12] Lufaso, M. W. & Woodward, P. M. (2001). Prediction of the crystal structures of perovskites using the software program SPuDS. Acta Cryst. B57, 725-738.